BURLEIGH DODDS SERIES IN AGRICULTURAL SCIENCE

# Understanding and preventing soil erosion

Edited by Dr Manuel Seeger, University of Trier, Germany


burleigh dodds
SCIENCE PUBLISHING

# Advances in modeling soil erosion risk

*Sudhanshu S Panda, University of North Georgia, USA; Debasmita Misra, University of Alaska Fairbanks, USA; Devendra M Amatya and Johnny M Grace III, USDA Forest Service, USA; and Anita Thompson, University of Wisconsin-Madison, USA*



## 1 Introduction

Evidence of climate change and its increasing impact on the environment and the erosion of soil has caught the attention of researchers globally. Soil erosion, considered as one of the worst geohazards human facing on the earth, is one of the environmental phenomena most affected by climate change. In the scientific community, there is a consensus that a critical impact of climate change is the increase in the quantity and intensity of precipitation (Giang et al.,

http://dx.doi.org/10.19103/AS.2023.0131.09

Chapter taken from: Seeger, M. (ed.), *Understanding and preventing soil erosion*, pp. 127–150, Burleigh Dodds Science Publishing, Cambridge, UK, 2024, (ISBN: 978 1 80146 379 9; www.bdspublishing.com)

2017). An increase in precipitation would lead to higher rates of soil erosion (Parry et al., 2007). Many studies (Zhang and Nearing, 2005; Zhang et al., 2005; Pruski and Nearing, 2002; Nearing, 2001; Giang et al., 2017; Almargo et al., 2017; Licciardello et al., 2019) examined the change of soil erosion in response to changing climate conditions using global climate models (GCMs) and confirmed an increase in the rate of soil erosion.

The United States Geological Survey (USGS) regional regression equations (Feaster et al., 2014; Wagner et al., 2016), the Rational Method (Kuichling, 1889), and the Soil Conservation Service–Curve Number (SCS-CN) method (NRCS, 2004) have been widely used to estimate design-storm peak discharge for different return intervals (ODOT, 2014). These methods are based on site-specific hydraulic characteristics that can be represented by simple watershed average parameters, i.e. runoff coefficient, curve number (CN), time of concentration, and basin characteristics (size, shape, topography, soils, geology, and land use) (Schwab et al., 1971).

Precipitation intensity–duration–frequency (PIDF) curves have been developed to take account of climatic factors (US Water Resource Council, 1981; Hrachowitz et al., 2013; Rogger et al., 2012). These PIDFs have connected the extreme precipitation storm event values that are now being observed worldwide (in the last few decades) with climate change (Amatya et al., 2021). The US National Oceanic and Atmospheric Administration (NOAA) Atlas 14-based gridded PIDF values (Bonnin et al., 2006; Perica et al., 2013) are available in raster format that uses regional frequency analysis using the L-moments method (Hosking and Wallis, 2005) with annual maximum and partial series storm events data from various weather stations managed by different government agencies in the United States. Although the precipitation data is not fully up-to-date, comprehensive historic records have been used in developing PIDFs (Panda et al., 2022). Researchers, engineers, and land managers in United States have the opportunity to make increasing use of climate change scenario storm (PIDF) data in soil erosion analysis (Panda et al., 2022).

Biassutti and Seager (2015) suggest that soil erosion has generated significant environmental, social and economic damage globally. The impact of climate change on soil erosion will severely affect all types of land cover, especially those with a steep topography. We are experiencing soil erosion in the form of landslides in many parts of the world as a consequence of climate change, with alternating La-Nina and El-Nino conditions (Moreiras et al., 2018). According to the United States Department of Agriculture (USDA) Forest Service (FS) (Rasmussen et al., 2018), nearly 200 million acres of public land are susceptible to a wide range of climate change impacts in every region of the country. The extreme rainfall events would cause potentially severe damage to the USDA-FS-managed road system in mountainous and less accessible terrains due to soil erosion (Panda et al., 2018, 2019; Amatya et al., 2017).

NOAA Atlas-14 sources probably do not use local data from long-term precipitation gauges on small headwater catchments located in several USDA-FS experimental forests and ranges (EFRs) (Amatya et al., 2019; Laseter et al., 2012; Moran et al., 2008). However, PIDF raster formatted data developed using surface interpolation algorithms for individual states of USA is quite useful in local soil erosion analysis (Panda et al., 2022). Developing modified soil erosion models using GCM supported by climate data are essential for watershed management and would pave way for identifying the best soil conservation measures for safeguarding many vulnerable engineering structures from soil erosion due to extreme weather events.

## 2 The development of the universal soil loss equation and revised universal soil loss equation models

USLE, the refined mathematical universal soil loss equation model, developed by Wischmeier and Smith (1965a,b), is the most commonly used model for predicting soil losses due to area erosion. The model is also useful in determining the adequacy of conservation measures in farm management planning and for predicting nonpoint sediment losses in pollution control programs. It is presented in algorithmic form as:

$$A = R \times K \times L \times S \times C \times P \quad (1)$$

where

| | |
|---|---|
| $A$ = | Computed soil loss per unit area |
| $R$ = | Rainfall factor: the number of erosion index units in the period of consideration. This is the measure of erosive force of specific rain. |
| $K$ = | Soil erodibility factor: the erosion rate/unit of erosion index for a specific soil, in a cultivated continuous fallow on a 9% slope and 22.1 m long. |
| $L$ = | Slope length factor: the ratio of soil loss from field slope length to that from a 22.1 m length on the same soil type and gradient. |
| $S$ = | Slope gradient factor: the ratio of soil loss from the field gradient to that from a 9% slope on the same soil type and slope length. |
| $C$ = | Cropping management factor: the ratio of soil loss from a field with specific cropping and management to that from the fallow condition on which K is evaluated. |
| $P$ = | Erosion control practice factor: the ratio of soil loss with contouring, strip cropping, or terracing to that with straight row farming, up and down slope. |

In the 1940s, A. W. Zingg (Zingg, 1940) introduced the first mathematical equation to estimate soil erosion losses in a field experiment based on natural and simulated rainfall using a Shelby loam soil in Missouri (USA). The equation is:

$$X = CS^mL^n \quad (2)$$

where $X$ is total soil loss from a land slope of unit width, $C$ is a constant of variation, $S$ is land slope (%), $L$ is horizontal length of land slope (ft), and $m$ and $n$ are empirical exponents.

Zingg (1940) then defined average soil loss per unit area from a slope of unit width represented by:

$$A = CS^mL^{n-1} \quad (3)$$

where the values of $m$ and $n$ (derived from the simulated rainfall experiment) are 1.4 and 0.6, respectively.

Smith (1941) modified Zingg's soil loss equation with the introduction of a factor, $P$, representing the ratio of soil loss with a mechanical conservation practice with respect to soil loss without the practice. The new equation by Smith (1941) used the same values of exponent $m$ and $n$ as developed by Zingg (1940) and presented it as:

$$A = CS^{1.4}L^{0.6}P \quad (4)$$

Smith's work established the concept of an allowable soil loss, now known as the 'T-Value' (tolerable soil loss value), based on maintenance of soil fertility (Laflen and Flanagan, 2013). Browning et al. (1947) and Musgrave (1947) later introduced a broad range of factors to account for in erosion estimation such as crop production, soil characteristics, and climate condition, paving the way for a more complete soil erosion equation.

Wischmeier and Smith (1965a,b) subsequently made available the first published USLE predicting rainfall–erosion losses from cropland east of the Rocky Mountains. USLE has been updated three times as:

- USLE (Wischmeier and Smith, 1978);
- Revised USLE (RUSLE) (Renard et al., 1997); and
- RUSLE2 (USDA-ARS, 2013).

The USLE, RUSLE, and RUSLE2 models, all follow the same equational concept of multiplying soil erosion-inducing spatial factors such as $R$ (rainfall erosivity factor), $K$ (soil erodibility factor), $L$ (slope length factor), $S$ (slope gradient factor), $C$ (cropping management factor), and $P$ (erosion control management factor) to obtain a computed soil loss per unit area.

Among those six factors, the $R$-factor is particularly important given the increasing occurrence of extreme storm events. Along with the modification of the $R$-factor, $L$- and $S$-factors can be modified with greater accuracy because of the availability of LiDAR-based topographic data. The LiDAR-based digital elevation model (DEM) would improve the accuracy of the $L$- and $S$-factors to quantify soil erosion correctly. The advent of unmanned aerial vehicle

(UAV)-based image acquisition and improved image segmentation algorithms is also paving way for more accurate *C*- and *P*-factor development. This chapter reviews developing a modified RUSLE model using ArcGIS ModelBuilder automation to develop processes for improving each USLE factor so that soil erosion quantification can be estimated more precisely in both temporal and spatial dimensions.

USLE has been integrated with geographic information system (GIS) data to estimate the amount of soil erosion from a watershed since the mid-1990s. GIS data helps users manipulate and analyze spatial data with ease and accurately identify spatial locations vulnerable to soil erosion (Yitayew et al., 1999; Ouyang and Bartholic, 2001; Lufafa et al., 2003; Panda et al., 2004).

The revised universal soil loss equation (RUSLE), a newer version of USLE, was developed by modifying it to estimate *R*-, *K*-, *C*-, and *P*-factors, as well as soil erosion, more accurately (Renard et al., 1991). The use of the ARC Macro Language (AML) program was not sufficiently fast in 1990s to spatially calculate the *LS*-factor (Panda et al., 2004). Van Remortel et al. (2004) developed an array-based C++ program to automate the calculation of the *LS*-factor from the DEM.

However, with the availability of the latest high-spatial soil data (gSSURGO, 10 m), *L*- and *S*-factor development has become easier. The *L*- and *S*-factors are available in three soil attributes (low depth, high depth, and representative) format in the gSSURGO characteristics (attributes) database. With the advent of graphical user interface (GUI)-based GIS software and advances ModelBuilder technology in GIS, it has become easier to develop RUSLE models to determine soil erosion rate from a watershed. Many researchers have used RUSLE models to estimate the amount of erosion from fields and watersheds (Renard et al., 1997; Millward and Mersey, 1999). However, few have used ArcGIS ModelBuilder to build a spatial model using the RUSLE equation to estimate soil erosion from a watershed (Sharma, 2008; Daggupati et al., 2009; Panagopoulos and Ferreira, 2010; Panda et al., 2022). The RUSLE model developed in the ArcGIS ModelBuilder environment has helped to automate the process.

## 3 Introducing the *R*-factor (rainfall factor) into universal soil loss equation/revised universal soil loss equation/revised universal soil loss equation 2

Wischmeier (1959) used precipitation and soil loss data from fallow plots to assess the role of rainfall in estimating storm soil loss. The rainfall-runoff erosivity factor (*R*) was developed as a measure of the erosion force of a specific rainfall event. The *R*-factor is calculated as the average annual summation ($EI_{30}$) values of the amount of rainfall from storms with no less than 1.27 cm (0.5 inch) in a normal precipitation year or with a maximum 15-min intensity >25.4 mm $h^{-1}$ (Wischmeier and Smith, 1978). In RUSLE, a longer storm period is divided into two storms when there is <0.13 cm (0.05 inch) during 6-h storm period (Yin et al., 2017). A monthly erosivity density map was developed in RUSLE2 using 15-min data from 3700 stations based on monthly precipitation data with a spatial resolution of 4 km obtained from the Parameter elevation Regression on Independent Slopes Model (PRISM, http://www.prism.oregonstate.edu/) database.

The *R*-factor represents the erosivity of climatic conditions at a particular location. Its average value has been determined from historical weather records. Wischmeier (1959) has evaluated the suitability of the *R*-factor at other locations (compared to the three experimental plot locations used in its development) for various cropping periods. The R-value proved to be effective for estimating rainfall-related soil loss (Laflen and Flanagan, 2013). By 1965 Isoerodent maps were available with the distribution of $EI_{30}$ for half-month periods for areas east of the Rocky Mountains (Wischmeier and Smith, 1965b). The publication also provided statistics related to probabilities of occurrence of single storms and single-year *R*-values for many locations in the USA.

It has been assumed that storm losses from rainfall are directly proportional to the product of the total kinetic energy of the storm (E) multiplied by its maximum 30-min intensity (IWR, 2002). The erosivity of an individual storm is computed as the product of the storm's total energy ($E$), which is closely related to storm amount, and the storm's maximum 30-min intensity ($I_{30}$). The *R*-factor represents the average storm $EI_{30}$ values over a year based on two key storm characteristics affecting erosivity: the amount of rainfall and peak intensity sustained over an extended period (IWR, 2002). However, with the exception of mean annual precipitation (P), $I_{30}$ data is not readily available for most geographic areas. As a result, *R*-factor estimates as a function of $P$ are often used since $P$ is a parameter that is available for most geographic regions of the world.

Wischmeier and Smith (1965a) developed the following empirical equation for determining the energy (E) required to initiate the motion of sediment particles:

$$E = 916 + 331 \log_{10} I_{30} \tag{5}$$

where $E$ is in foot-tons per inch (23.11 metric tons $mm^{-1}$) and $I$ is the intensity of the storm in inches per hour (25.4 mm $h^{-1}$).

They found that, for a given storm, energy did not increase with intensity above 3 in $h^{-1}$, so the maximum value used for in this equation is 3 in $h^{-1}$. The $E$ value was determined from the storm intensity ($I$) values and $I_{30}$ values for each individual storm over the period of record. The product of $I$ and $I_{30}$ was calculated, summed, and averaged annually over the period of record to provide the *R*-factor as represented by:

$$R = \frac{1}{n}\sum_{j=1}^{n}\left[\sum_{k=1}^{m}(E)I_{30k}\right] \tag{6}$$

where $k$ is the number of the individual storms to a total of $m$ storms in a year, and $j$ represents the year up to the total number of years, $n$, over which data was collected.

Renard et al. (1997) published the RUSLE with a new method to determine $R$-factor. However, they still used the EI parameter and the summation/averaging equation detailed above with $I_{30}$ determination in the same manner as suggested by Wischmeier and Smith (1965a). However, $E$ values were determined using an alternative equation given as:

$$E = \sum_{k=1}^{n} e_r v_r \tag{7}$$

where $e_r$ is the rainfall energy per unit depth of rainfall per unit area (foot-tons per acre per inch = 9.25 metric tons ha$^{-1}$ mm$^{-1}$), $v_r$ is the depth of rainfall in inches for the $r$th increment of a storm hyetograph which is divided into $m$ parts, each with essentially constant rainfall intensity (inch h$^{-1}$).

For each increment of the storm, $e_r$ is determined using the following equation:

$$e\mathrm{r} = 1099\ [1-0.072^{(-.27}\mathrm{ir}^{)}] \tag{8}$$

where $i_r$ is the approximated constant intensity over the time increment. The value of $v_r$ is calculated by the following:

$$v_r = i_r \times t_r \tag{9}$$

Other parts of the world may not have PIDF raster data to develop a $R$-factor or isoerodent map. Rainfall data is available in most developing countries but is obtained from non-recording-type rain gauges. This means that little quantitative information is available on the magnitude of instantaneous intensity (i.e. for 30 min) and the energy of a rain storm for a longer period. As a result, simple empirical formula for estimating the rainfall erosivity index ($R$-factor) from rainfall amounts is used. Petebendege (1990) has found a relationship between the 'mean annual erosivity', 'mean annual rainfall', and 'rainfall aggressive index' by multivariable regression analysis. The equation derived is as follows.

$$\mathrm{MAE} = (5.62 \times \mathrm{MAR}) + (92.32 \times \mathrm{RA}) - 11754.49 \tag{10}$$

where MAE = mean annual erosivity (in J km$^{-2}$)

MAR = mean annual rainfall (in mm)

RA = rainfall aggressiveness index

## 4 Introducing the *K*-factor (soil erodibility factor) into universal soil loss equation/revised universal soil loss equation/revised universal soil loss equation 2

Auerswald et al. (2014) have reviewed how the soil erodibility factor (*K*-factor) was developed by Wischmeier and Smith (1965a) and its subsequent development. In the UK, the *K*-factor as an attribute is available with gSSURGO data. However, setting up and collecting data from experimental runoff plots to establish the *K*-factor is expensive and time consuming. Many developing countries lack even simple soil data (Panda et al., 2004). In these cases, the *K*-factor can be developed using the Nomograph process that uses five factors of soil (calculated as percentages):

- Silt + very fine sand (0.002−0.10 mm);
- Sand (0.10−2.0 mm);
- Organic matter;
- Soil structure; and
- Permeability.

The soil erodibility factor '*K*' can be evaluated on experimental plots using the following equation:

$$K = A/\text{RLSCP (for non-standard conditions)} \quad (11)$$

$K = A/R$ (for standard condition i.e. slope gradient = 9%, slope length = 22.1 m, cultivated continuous fallow land and ploughing up and down the slope. Here L = S = C = P = 1 ) (12)

## 5 Introducing the *L*-factor (slope length factor) and the *S*-factor (slope gradient factor) into universal soil loss equation/revised universal soil loss equation/revised universal soil loss equation 2

Slope length is defined as 'the distance from the point of origin of over land flow to either:'

- The point where the slope decreases to the extent that depositions begins; and
- The point where the run off enters a well-defined channel that may be a part of drainage network or a constructed channel.

The slope length factor (*L*) is defined as:

$$L = (\lambda/22.1\ )m \quad (13)$$

where $\lambda$ = field slope length (in m)

$m$ = exponent influenced by the interaction of slope length with gradient and may be influenced by the soil properties and the type of vegetation.

= 0.3 (for long slopes with gradient <0.5%)

= 0.6 (for slope gradient >10%)

= 0.5 (the mostly acceptable average value)

The United States Soil Conservation Service (US-SCS) (1972) developed an equation modifying the slope gradient parameter determining formula of Wischmeier (1959). The equation in its modified form is given as:

$$S = (0.43 + 0.30\,s + 0.043\,s^2)/6.613 \quad (14)$$

where $s$ = slope gradient (in %)

This slope gradient equation was modified by Wischmeier and Smith (1978) to a form of slope gradient related to the slope steepness in 'degree' form. The equation is as illustrated in Equation 15. This equation was established using numerous test plot experiments:

$$S = 65.41\sin^2\theta + 4.56\sin\theta + 0.065 \quad (15)$$

where $S$ = slope gradient factor and $\theta$ = angle of slope in degrees

The US-SCS (1972) developed an equation to account for the combined effect of slope length and slope gradient on soil loss. The equation holds good for slope gradient up to 20% and field slope length of up to 350 m:

$$LS = \sqrt{\lambda\left(0.0138 + 0.00965s + 0.00138s^2\right)} \quad (16)$$

where $\lambda$ = measured slope length in the field, $s$ = slope gradient in percentage

The equation for '*LS*'-factor calculation for slope gradient from 10% to 50% and slope length up to 800 m is as follows:

$$\mathrm{LS} = (\lambda / 22.1)0.6\,(\mathrm{s} / 9)1.4 \quad (17)$$

where $\lambda$ = measured slope length in the field, $s$ = slope gradient in percentage

The US-SCS (1972) has developed a methodology for calculating the combined '*LS*'-factor for all kinds of slopes and slope lengths. The equation is represented as:

$$LS = \sqrt{\lambda / 100\left(0.136 + 0.097s + 0.0139s^2\right)} \quad 18$$

where $\lambda$ = measured slope length in the field, $s$ = slope gradient in percentage

A newly modified equation combining '*L*-' and '*S*'-factor can be used for all conditions of slope length and gradient:

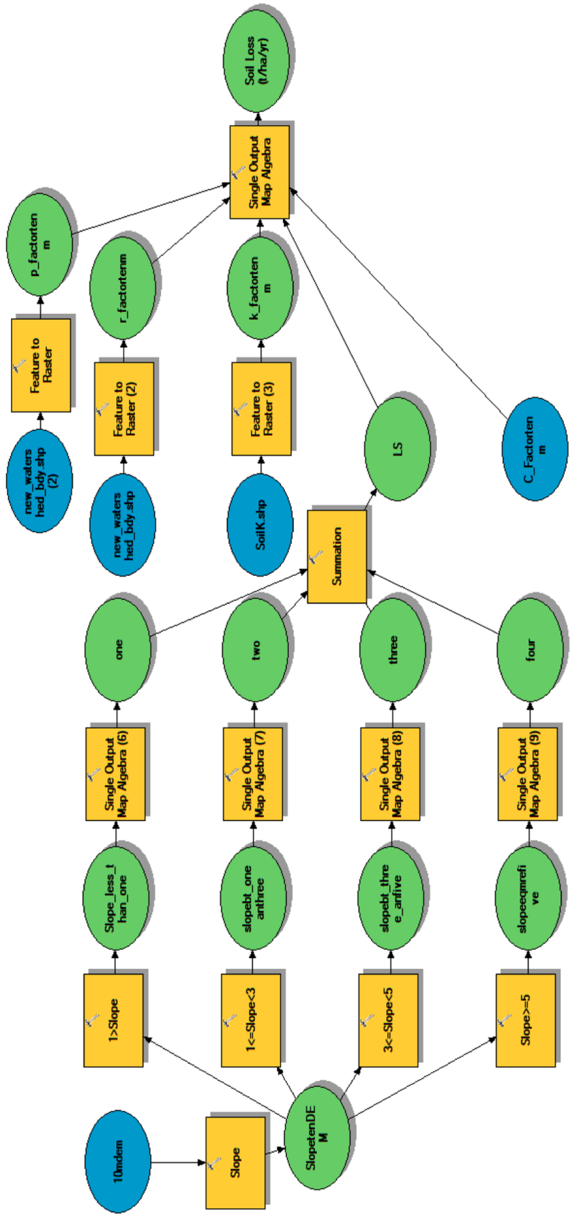


**Figure 1** Automated geospatial model developed to calculate annual soil erosion load to Lake Nickerboker (Ada Creek retention pond), an example.

$$LS = (\lambda/22.13)m\ [65.41 \sin^2\theta + 4.56 \sin\theta + 0.065] \quad (19)$$

where $\lambda$ = measured slope length in the field, $\theta$ = angle of slope in degrees, $m$ = exponent factor varying from 0.2 to 0.5 and mostly 0.5 is used.

More recently the *LS*-factor has been calculated using the formula:

$$LS = [0.65 + 0.456\ (slope) + 0.00654\ (slope)^2\ ]\ (98.4/72.5)^{NN} \quad (20)$$

where NN is 0.2 for slope less than 1%, 0.3 if slope is between 1% and 3%, 0.4 if slope is between 3% and 5%, or 0.5 for slopes greater than 5% that can be implemented in ArcGIS ModelBuilder (Panda et al., 2011).

Individual slope raster data can be created by selecting cell values of less than 1%, between 1% and 3%, between 3% and 5%, and slopes greater than 5% using the classified slope raster of the study area as shown in Fig. 1. Each slope raster gets transformed into the individual LS raster through the use of 'Map Algebra' tool, which can multiply the raster cell values with the LS equation shown in Equation 20. For each slope raster, the NN value is changed according to the corresponding values of 0.2, 0.3, 0.4, or 0.5. Once all four LS rasters are created, they are summed (spatially) together using the 'Sum' tool available with the Math Toolset of Spatial Analyst Toolbox of ArcToolbox (Fig. 1). Geospatial modelbuilders can obtain the final *LS*-factor raster using this method in ArcGIS. Separate *L*- and *S*-factors are also available separately as attributes for most parts of USA via gSSURGO or STASGO2 data. USDA developed gSSURGO (10m spatial resolution Gridded SSURGO raster) data contains L- (Slope Length - USLE) and S- (Slope Gradient - USLE) factors to be directly embedded to the Modified RUSLE model. However, it is not available for other parts of the world. Researchers should rely on the above L-, S-, or LS-factor development algorithms presented above.

## 6 Introducing the *C*-factor (cropping/cover management factor) and the *P*-factor (area control practice factor) into universal soil loss equation/revised universal soil loss equation/revised universal soil loss equation 2

The cropping/cover management (*C*) factor describes the total effect of vegetation, residue, soil surface, and management on soil loss. The value is typically not constant over the year. Although treated as an independent variable in the equation, the true value of this factor is potentially dependent upon all other factors. Hence the value of the '*C*'-factor needs to be established experimentally in local conditions. Land cover classified maps help to obtain a spatial *C*-factor using *C*-factor tables (database) developed by a wide range of researchers (see review in Gabriels et al., 2003). Panda et al. (2022) have developed a *C*-factor in ArcGIS ModelBuilder using the NDVI-based formula

$\left(C = 0.1\left(\frac{NDVI + 1}{2}\right)\right)$, and a *P*-factor using the classified land-use map of the study area with the combination of NDVI classification and land conservation spatial data available for the study area. It is to be noted that many country's (including United States) catalog all conservation lands as GIS vector layers and they can be used for P-factor raster development along with vegetation density information obtained from NDVI classification raster.

## 7 Case study: using high spatial resolution precipitation data for *R*-factor estimation

Rasterized rainfall data, such as PRISM data from a 4-km grid, were first introduced in *R*-factor calculation for RUSLE2 in the 1990s (Daly et al., 1997). *R*-factor values can be computed accurately on a spatial (grid) basis with the latest weather based $I_{30}$ data availability in <1 km$^2$ (~800 m × 800 m) grid format via the NOAA (http://hdsc.nws.noaa.gov/hdsc/pfds/pfds_gis.html) (Bonnin et al., 2006). This improvement represents a leap forward in estimation. With these data, Equations 4 and 5 can easily be replicated with the grid-based (raster) $I_{30}$ and $I$ data to produce timely *R*-factor for regions of USA. The *R*-factor calculation is potentially more accurate given the availability of recent precipitation data. Developing the *R*-factor and subsequent isoerodent map development could be facilitated by geospatial technology-based model development since precipitation records are available in raster format.

### *7.1. National Oceanic and Atmospheric Administration precipitation raster data format and description*

The data used in this study (the State of Georgia as the study area, Fig. 2) for the *R*-factor calculation are the same 100-year, 30-min storm event raster data developed by NOAA, NWS HDSC which makes *R*-factor development more efficient with independent *R*-values calculated for each 0.64 km$^2$ grid or pixel. Metadata for storm event ($I_{30}$) data suggests that these data are extremely efficient for developing the *R*-factor for the US conditions The storm event raster was developed using precipitation records from the 250+ National Climatic Data Center (NCDC) stations collected at 15-min intervals, six Georgia Forestry Commission (GFC), Fire Weather System (FWS) stations at hourly intervals, four Remote Automatic Weather Stations (RAWS) stations at hourly intervals, two Fort and Voluntary Observers Database (FORTS) stations at hourly intervals, and one USGS station at hourly intervals (Perica et al., 2013).

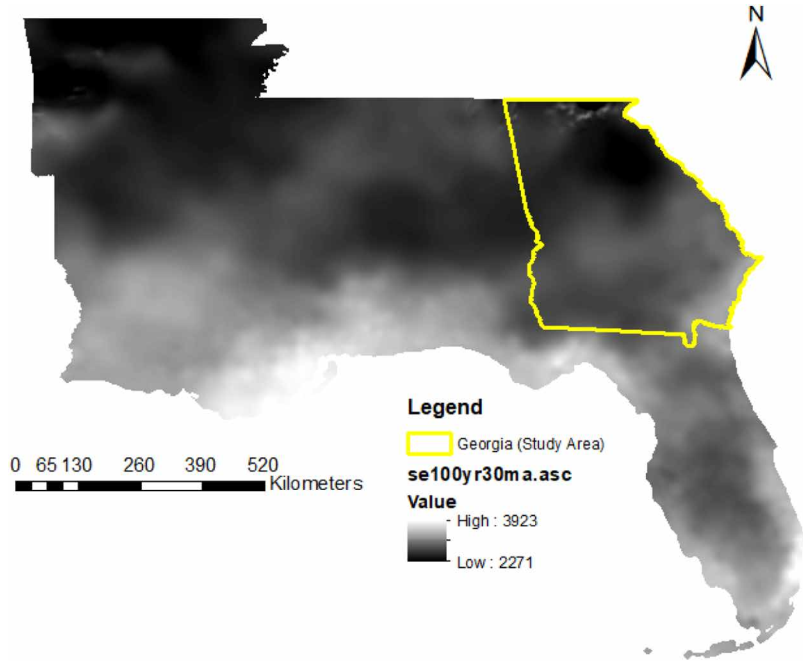


**Figure 2** Partial duration series 100-year, 30-min precipitation frequency raster of southeastern USA. The study which is within the state boundary for Georgia, USA is outlined in yellow. Source: Adapted from: Datahttps://www.nws.noaa.gov/oh/hdsc/PF_documents/Atlas14_Volume9.pdf .

### *7.2. Isoerodent map development using National Oceanic and Atmospheric Administration precipitation raster*

This study for estimating the *R*-factor covered the State of Georgia in the United States of America (USA). The raster file (se100yr30ma.asc) covering southeastern US (Fig. 2) was downloaded from https://www.nws.noaa.gov/oh/hdsc/PF_documents/Atlas14_Volume9.pdf (NOAA, 2019). This represents a partial duration series precipitation frequency analysis of 100-year average recurrence interval with 30-min duration data. The raster data is of 0.64 km$^2$ spatial resolution and according to NOAA (2019), '*these precipitation frequency (PF) estimates are used as basic design criteria for a wide variety of hydraulic structures such as culverts, roadway drainages, bridges and small dams. This dataset is for the display and/or analyses of spatially distributed point PF estimates*'. The weather data used for the $I_{30}$ raster development ranges from as early as second decade of the twentieth century until the latest in 2011 (Perica et al., 2013). Annual average precipitation data (1980–2010) for Georgia, USA

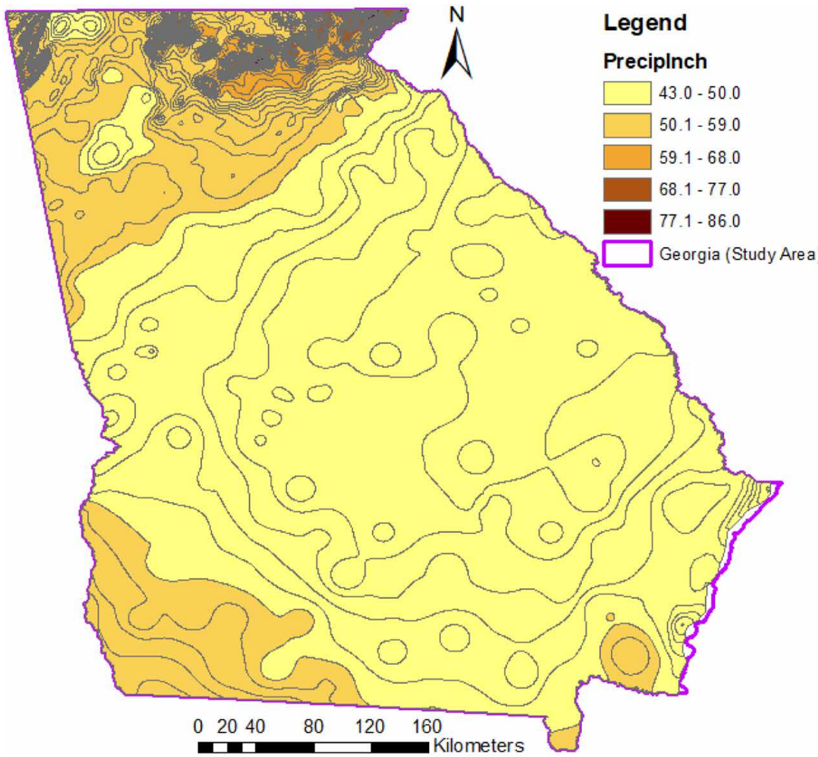


**Figure 3** Annual average precipitation distribution vector of Georgia. Source: Adapted from: https://datagateway.nrcs.usda.gov/.

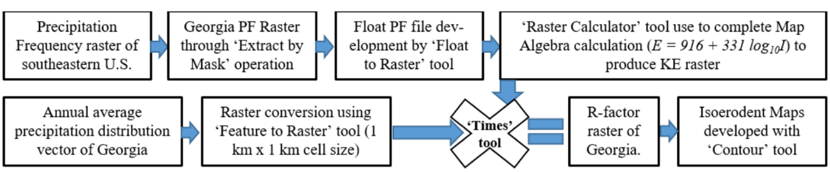


**Figure 4** Basic procedural flow chart for *R*-factor and isoerodent map development for Georgia using NOAA PF raster and the average annual precipitation distribution vector.

was downloaded in vector format (Fig. 3) from the USDA NRCS Geospatial Data gateway (https://datagateway.nrcs.usda.gov/). The data was available at the same 0.64 $km^2$ spatial resolution grid (raster) using the 'precipitation in inch' attribute to suit to the spatial resolution of NOAA PF data for Georgia, USA. Step-by-step processes (Fig. 4) were followed as directed by the web interface to obtain the *R*-factor raster and subsequent isoerodent map of different unit intervals for Georgia.

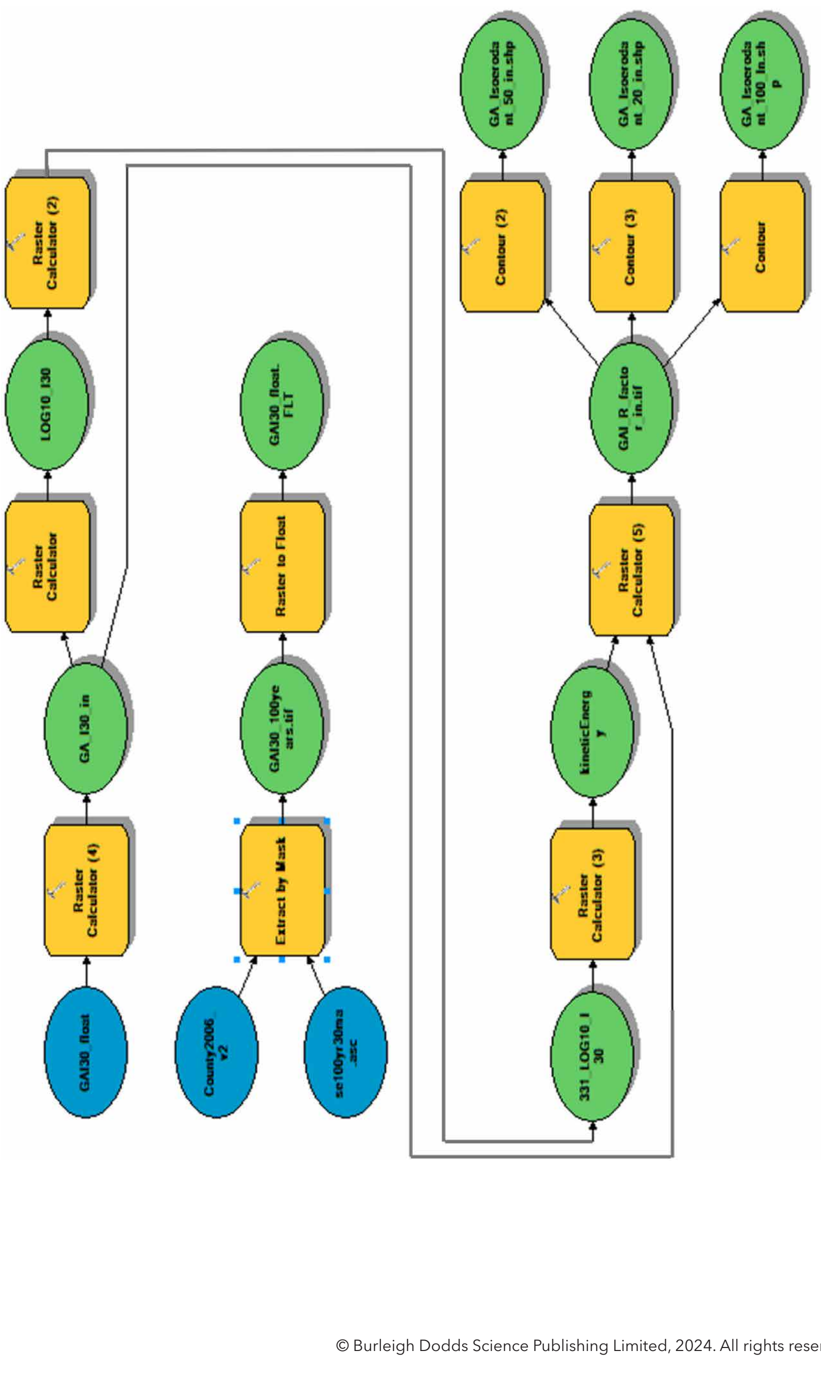


**Figure 5** Automated geospatial model framework for obtaining *R*-factor raster and isoerodent maps vector of Georgia.

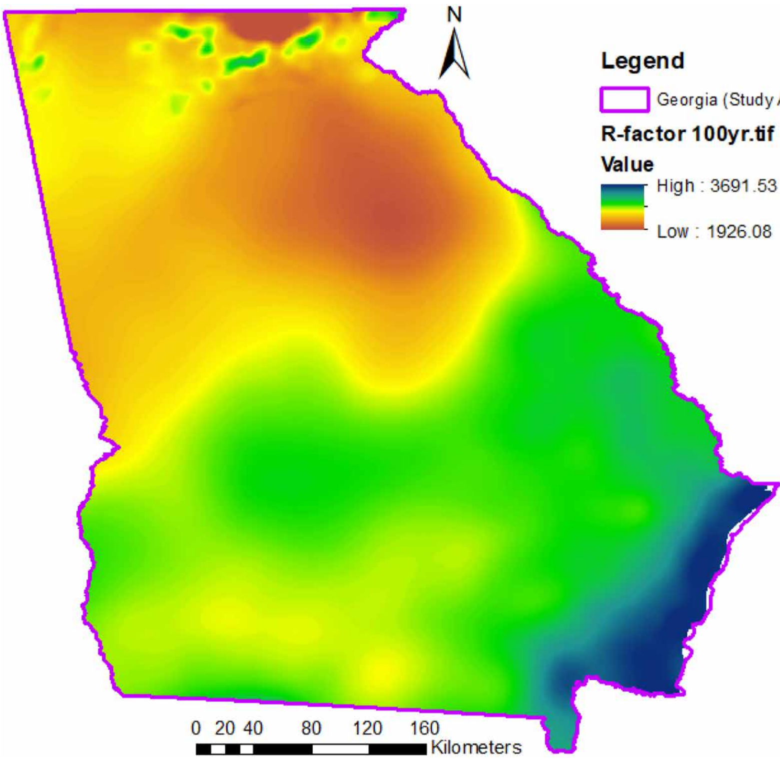


**Figure 6** *R*-factor map of Georgia developed with latest NOAA developed precipitation frequency.

A Georgia USA shapefile was used as mask with the se100 year 30-min raster data to produce the study area [the area of interest (AOI)] PF raster which was subsequently converted to a float file to facilitate raster calculation (Map Algebra) with ArcGIS 10.5 software (Fig. 5). This float file served as the primary input for the rest of the automated geospatial model developed in the ArcGIS ModelBuilder platform. The input float file was used as input for *I* in the equation '$E = 916 + 331 \log_{10} I$' in ArcGIS 'Raster Calculator' tool with proper algebraic function input. In order to make the overall raster calculation process smoother and efficient, a series of rasters, which included $\log_{10} I$, $331 \log_{10} I$, and $916 + 331 \log_{10} I$ rasters, were developed. The final raster developed was the kinetic energy (*E*) raster. The *E* raster was multiplied by the Georgia, USA, annual average precipitation raster to account for Equation 5 of Wischmeier and Smith (1965a,b). We were thus able to develop a new Georgia USA *R*-factor raster (Fig. 6).

Isoerodent maps of Georgia, USA, at various intervals, i.e. 100 m (Fig. 7a), 50 m (Fig. 7b), and 20 m (Fig. 7c), respectively, were developed using the contour tools described earlier. This makes it possible to generate erosion index values

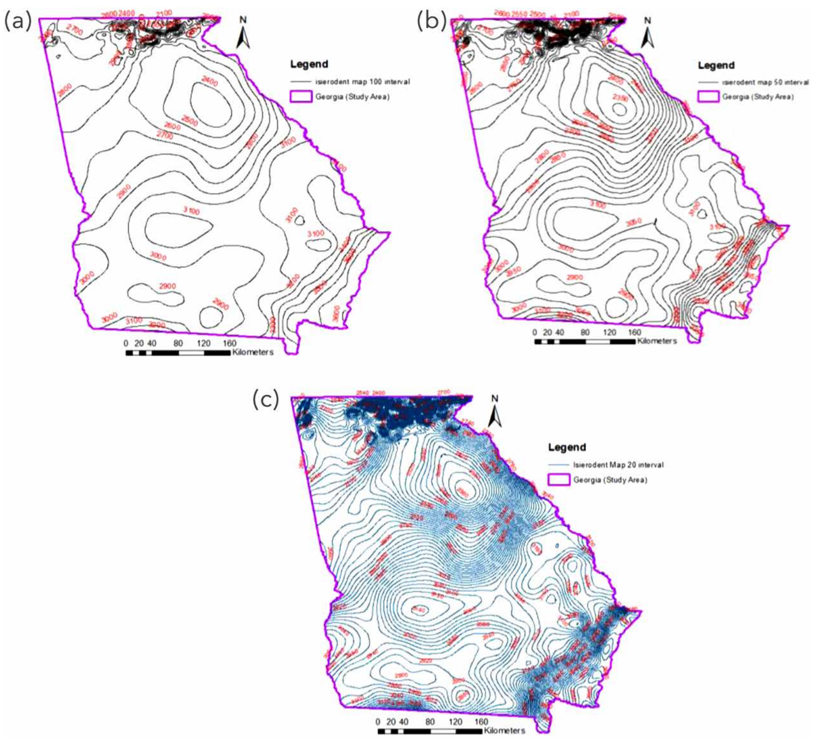


**Figure 7** Isoerodent map of Georgia at 100 (a), 50 (b), and 20 (c) unit interval developed with latest NOAA developed precipitation frequency data.

for a smaller spatial extent for soil erosion quantification. However, the *R*-factor will then be unique for a ~0.7 km$^2$ grid or pixel based on the NOAA spatial rasters used in this study. Finally, the isoerodent results from our study were compared with the old isoerodent map of Georgia, USA (Fig. 8). The *R*-factor calculated with latest climate NOAA raster data produced high erosion index (*R*-factor) values, i.e. ~six to seven times higher than the earlier isoerodent map for Georgia.

## 8 Conclusion and future trends

Individual geospatial models for *K*-, *L*-, and S-factors are being developed using gSSURGO soil data. *C*- and *P*-factors are being developed in the ArcGIS ModelBuilder using satellite remote sensing data and a normalized difference vegetative index (NDVI) approach with updated algorithms that comply with the latest changes in land use and conservation practices.

In cold climates, where frost forms during the winter season in the soil and where areas are also experiencing increasing amounts of snow precipitation due to climate change, the RUSLE model needs to be modified significantly in

**Figure 8** Current isoerodent map of eastern USA (EPA, 2001).

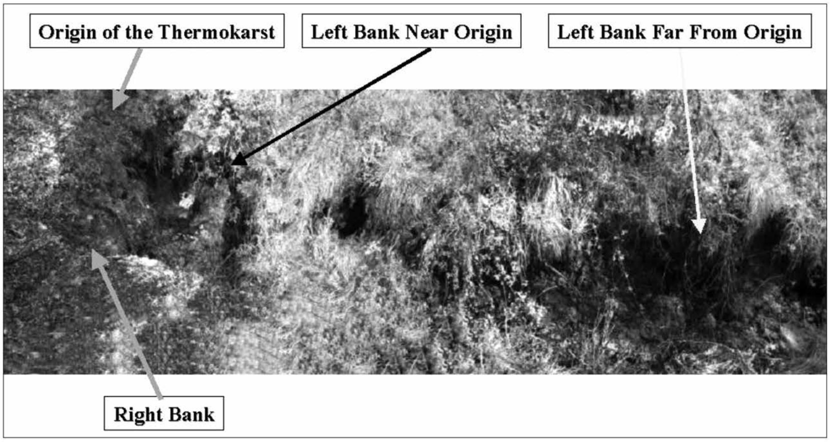


**Figure 9** Photograph of a typical thermokarst from the Caribou-Poker Creek Watershed of Alaska.

order to quantify the amount of erosion or erodibility of these areas. In Arctic and the sub-Arctic regions, such as Alaska, the soil is prone to erodibility due to snowmelt and/or melting of permafrost-forming thermokarsts (see Fig. 9; Misra et al., 2011). Thermokarsts are formed when the permafrost melts and induces thaw slump. The loose slumped or collapsed soil is then eroded due to surface rainfall, subsequent snowmelt or groundwater pressure. The snowmelt erosion is only possible when the shear force exerted by the snowmelt exceeds the soil matrix strength bounded by the soil frost (Daanen et al., 2011). This is also true for soil erosion in Wisconsin or other northern cold climate regions of the USA.

As noted earlier, the new *R*-factor values established through the case study differ from the old isoerodent map of Georgia. NOAA uses current precipitation data (through to 2013 and many spatial cases through 2019) which better reflect recent shifts in precipitation patterns. Since they were not able to do this, the authors recognize the need for verification of the *R*-factors developed by this procedure with field experimentation. The goal of the case study was to develop an automated model for efficiently developing latest *R*-factors of any spatial locations using PF rasters created by NOAA. The authors are applying this technique in three large watersheds in a forthcoming publication on 'streambank erosion vulnerability assessment (SBEVA) and RUSLE modeling supported forest structure vulnerability analysis and decision support.' This paper has been published in the journal *Environmental Modeling and Software* (Panda et al., 2022).

## 9 Acknowledgement

The authors would like to acknowledge the USDA Forest Service Southern Research Station (SRS) and Region 8 for funding the Georgia-based study. Furthermore, the authors extend thanks to the reviewers and editorial board members for this manuscript's review and publication.

## 10 References

Almagro, A., Oliveira, P. T. S., Nearing, M. A. and Hagemann, S. (2017). Projected climate change impacts in rainfall erosivity over Brazil. *Scientific Reports* 7(1), 8130.

Amatya, D. M., Sun, G. and Panda, S. S. (2017). Ecohydrological studies at Santee experimental forest, baseline data, extreme events, and hydrological vulnerabilities in the context of south Eastern US forests. Closing Keynote presented in the 2017 Municipal Wet Weather Stormwater Conference May 17, 2017, Charleston, SC.

Amatya, D. M., Tian, S., Marion, D. A., Caldwell, P., Laseter, S., Youssef, M. A., Grace, J. M.,Chescheir, G. M., Panda, S. S., Ouyang, Y., Sun, G. and Vose, J. M. (2021). Estimates of precipitation IDF curves and design discharges for road-crossing drainage structures: case study in four small forested watersheds in the Southeastern US.

*Journal of Hydrologic Engineering* 26(4), 05021004. DOI: 10.1061/(ASCE)HE.1943-5584.0002052. © 2021 American Society of Civil Engineers.

Amatya, D. M., Williams, T. M., Nettles, J. E., Skaggs, R. W. and Trettin, C. C. (2019). Comparison of hydrology of two Atlantic coastal plain forests. *Transactions of the ASABE* 62(6), 1509–1529.

Auerswald, K., Fiener, P., Martin, W. and Elhaus, D. (2014). Use and misuse of the K factor equation in soil erosion modeling: an alternative equation for determining USLE nomograph soil erodibility values. *CATENA* 118, 220–225.

Biasutti, M. and Seager, R. (2015). Projected changes in US rainfall erosivity. *Hydrology and Earth System Sciences* 19(6), 2945–2961.

Bonnin, G. M., Martin, D., Lin, B., Parzybok, T., Yekta, M. and Riley, D. (2006). Precipitation-frequency atlas of the United States. *NOAA Atlas* 14(2), 1–65.

Browning, G. M., Parish, C. L. and Glass, J. (1947). A method for determining the use of limitations of rotation and conservation practices in the control of soil erosion in Iowa. *Journal of the American Society of Agronomy*. 39(1), 65-73.

Daanen, R. P., Misra, D. and Thompson, A. (2011). Frozen soil hydrology. In: Haritashya, U. K., Singh, V. and Singh, P. (Eds) *Encyclopedia of Snow, Ice, and Glaciers*. Springer Press, USA. Part 6, 306–311.

Daggupati, P., Sheshukov, A., Douglas-Mankin, K. R., Barnes, P. L. and Delvin, D. L. (2009). Field-scale targeting of cropland sediment yield using ArcSWAT. In: Proceedings of the 5th International SWAT Conference, Boulder, CO, August 5–7, 2009.

Daly, C., Taylor, G. and Gibson, W. (1997). The PRISM approach to mapping precipitation and temperature. In: Proceedings of the 10th Conference on Applied Climatology, Reno, NV, October 20–24, 1997. Am. Table 4 continued from previous page.Meteorological Society, Boston, MA, pp. 20–23.

Feaster, T. D., Gotvald, A. J. and Weaver, J. C. (2014). *Methods for Estimating the Magnitude and Frequency of Floods for Urban and Small, Rural Streams in Georgia, South Carolina, and North Carolina, 2011*. United States Geological Survey, Columbia.

Gabriels, D., Ghekiere, G., Schiettecatte, W. and Rottiers, I. (2003). Assessment of USLE cover-management C-factors for 40 crop rotation systems on arable farms in the Kemmelbeek watershed, Belgium. *Soil and Tillage Research* 74(1), 47–53.

Giang, P. Q., Giang, L. T. and Toshiki, K. (2017). Spatial and temporal responses of soil erosion to climate change impacts in a transnational watershed in Southeast Asia. *Climate* 5(1), 22.

Hosking, J. R. M. and Wallis, J. R. (2005). *Regional Frequency Analysis: An Approach Based on L-Moments*. Cambridge University Press, UK.

Hrachowitz, M., Savenije, H., Blöschl, G., McDonnell, J., Sivapalan, M., Pomeroy, J. W., Arheimer, B., Blume, T., Clark, M. P., Ehret, U., Fenicia, F., Freer, J. E., Gelfan, A., Gupta, H. V., Hughes, D. A., Hut, R. W., Montanari, A., Pande, S., Tetzlaff, D., Troch, P. A., Uhlenbrook, S., Wagener, T., Winsemius, H. C., Woods, R. A., Zehe, E. and Cudennec, C. (2013). A decade of Predictions in Ungauged Basins (PUB)—a review. *Hydrological Sciences Journal* 58(6), 1198–1255.

Kuichling, E. (1889). The relation between the rainfall and the discharge of sewers in populous districts. *Transactions of the American Society of Civil Engineers* 20(1), 1–56.

Laflen, J. M. and Flanagan, D. C. (2013). The development of US soil erosion prediction and modeling. *International Soil and Water Conservation Research* 1(2), 1–11.

Laseter, S. H., Ford, C. R., Vose, J. M. and Swift, L. W. (2012). Long-term temperature and precipitation trends at the Coweeta Hydrologic Laboratory, Otto, NC, USA. *Hydrology Research* 43(6), 890–901.

Licciardello, F., Ciampalini, R., Pastor, A., Huard, F., Follain, S., Crabit, A., Le Bissonnais, Y. and Raclot, D. (2019, January). Modelling the impact of climate change and land use on soil erosion in a Mediterranean catchment. *Geophysical Research Abstracts* 21, P1-1, 1.

Lufafa, A., Tenywa, M. M., Isabirye, M., Majaliwa, M. J. G. and Woomer, P. L. (2003). Prediction of soil erosion in a Lake Victoria basin catchment using a GIS-based universal soil loss model. *Agricultural Systems* 76(3), 883–894.

Millward, A. A. and Mersey, J. E. (1999). Adapting the RUSLE to model soil erosion potential in a mountainous tropical watershed. *CATENA* 38(2), 109–129.

Misra, D., Daanen, R. P. and Thompson, A. (2011). Thermokarst. In: Haritashya, U. K., Singh, V. and Singh, P. (Eds) *Encyclopedia of Snow, Ice, and Glaciers*. Springer Press, USA. Part 19, 1158–1166.

Moran, M. S., Peters, D. P. C., McClaran, M. P., Nichols, M. H. and Adams, M. B. (2008). Long-term data collection at USDA experimental sites for studies of ecohydrology. *Ecohydrology* 1(4), 377–393.

Moreiras, S. M., Pont, I. V. D. and Araneo, D. (2018). Were merely storm-landslides driven by the 2015–2016 Niño in the Mendoza River valley? *Landslides* 15(5), 997–1014.

Musgrave, G. W. (1947). The quantitative evaluation of factors in water erosion: a first approximation. *Journal of Soil and Water Conservation* 2, 133–138.

Nearing, M. A. (2001). Potential changes in rainfall erosivity in the United States with climate change during the 21st century. *Journal of Soil and Water Conservation* 56, 229–232.

NOAA (2019). NOAA atlas 14 precipitation frequency estimates in GIS compatible format. Available at: https://hdsc.nws.noaa.gov/hdsc/pfds/pfds_gis.html. Alabama, Georgia Isopluvials of 1-Year 60-Minute Precipitation in Inches NOAA Atlas 14 Volume 9, Version 2. *Southeastern States* (2nd edn., Volume 14), National Oceanic and Atmospheric Administration, United States, 2013. Accessed on April 16, 2019.

NRCS (2004). *National Engineering Handbook: Part 630—Hydrology*, United States Department of Agriculture Soil Conservation Service, Washington, DC.

ODOT (2014). Roadway drainage manual, Chapter 7. In: *Hydrology*. Oklahoma Department of Transportation. Available at: https://www.ok.gov/odot/documents/Chapter%207%20Hydrology.pdf. Accessed on August 4, 2022.

Ouyang, D. and Bartholic, J. (2001). Web-based GIS application for soil erosion prediction. In: Proceedings of an International Symposium—Soil Erosion Research for the 21st Century Honolulu, HI, January 3–5.

Panagopoulos, T. and Ferreira, V. 2010, July. Decision support system for erosion risk assessment. In: Proceedings of the 14th WSEAS International Conference on Systems: Part of the 14th WSEAS CSCC Multiconference (Volume I, pp.76–80). World Scientific and Engineering Academy and Society (WSEAS).

Panda, S. S., Amatya, D., Grace, J. M., Caldwell, P. and Marion, D. (2018). Automated geospatial model based assessment of erosion vulnerability at forest road/ Stream crossings under extreme precipitation intensities scenario. Accepted to be published in the Proceedings and be presented in the Sixth Interagency Conference on Research in the Watersheds (ICRW) at National Conservation Training Center, Shepherdstown, WV, July 23–26, 2018.

Panda, S. S.,Amatya, D., Grace, J. M., Caldwell, P. and Marion, D. (2019). Forest road/stream crossings erosion vulnerability assessment using geospatial hydrologic model under extreme precipitation events. Presented in the 2019 American Geophysical Union (AGU) Conference, San Francisco, CA, December 9–13, 2019.

Panda, S. S., Amatya, D. M., Grace, J. M., Caldwell, P. and Marion, D. A. (2022). Extreme precipitation-based vulnerability assessment of road-crossing drainage structures in forested watersheds using an integrated environmental modeling approach.*Environmental Modelling and Software*, 105413. DOI: 10.1016/j.envsoft.2022.105413.

Panda, S. S., Andrianasolo, H., Murty, V. V. N. and Nualchawee, K. (2004). Forest management planning for soil conservation using satellite images, GIS mapping, and soil erosion modeling. *Journal of Environmental Hydrology* 12(13), 1–16.

Parry, M. L., Canziani, O. F., Palutikof, J. P., van der Linden, P. J. and Hanson, C. E. (2007). *Climate Change 2007: Working Group II: Impacts, Adaptation and Vulnerability*. Cambridge University Press, Cambridge.

Perica, S., Martin, D., Pavlovic, S., Roy, I., St Laurent, M., Trypaluk, C., Unruh, D., Yekta, M. and Bonnin, G. (2013). *NOAA Atlas 14 Precipitation-Frequency Atlas of the United States*, National Oceanic and Atmospheric Administration, Silver Spring, MD.

Perica, S., Pavlovic, S., Laurent, M. S., Trypaluk, C., Unruh, D., Martin, D. and Wilhite, O. (2013). *NOAA Atlas 14: Precipitation Frequency Atlas of the United States Volume 10: Northeastern States*. NOAA, National Weather Service, Silver Spring, MD.

Pruski, F. F. and Nearing, M. A. (2002). Climate-induced changes in erosion during the 21st century for eight U.S. locations. *Water Resources Research* 38(12), 1298.

Renard, K. G., Foster, G. R., Weesies, G. A., McCool, D. K. and Yoder, D. C. (1997). Predicting rainfall erosion by water: a guide to conservation planning with the revised universal soil loss equation (RUSLE). In: *Agriculture Handbook*, No. 703. US Government Printing Office, Washington, DC.

Renard, K. G., Foster, G. R., Weesies, G. A. and Porter, J. P. (1991). RUSLE: revised universal soil loss equation. *Journal of Soil and Water Conservation* 46(1), 30–33.

Rogger, M., Kohl, B., Pirkl, H., Viglione, A., Komma, J., Kirnbauer, R., Merz, R. and Blöschl, G. (2012). Runoff models and flood frequency statistics for design flood estimation in Austria–do they tell a consistent story? *Journal of Hydrology* 456, 30–43.

Schwab, G. O., Frevert, R. K., Barnes, K. K. and Edminster, T. W. (1971). *Elementary Soil and Water Engineering*, John Wiley & Sons, Inc., New York, 316 p.

Sharma, J. B. (2008). Erosion and sediment modeling of the Lake Lanier watershed. Ph.D. Thesis, Department of Geography, University of Georgia, Athens, GA, p. 187.

Smith, D. D. (1941). Interpretation of soil conservation data for field use. *Agricultural Engineering* 22, 173–175.

USDA–ARS (2013). *Science Documentation: Revised Universal Soil Loss Equation, Version 2*. USDA–ARS, Washington, DC.

US Water Resource Council (1981). Estimating peak flow frequencies for natural ungaged watersheds.

Van Remortel, R. D., Maichle, R. W. and Hickey, R. J. (2004). Computing the LS Factor for the revised universal soil loss equation through array-based slope processing of digital elevation data using C++ executable. *Computers and Geosciences* 30(9–10), 1043–1053.

Wagner, D. M., Krieger, J. D. and Veilleux, A. G. (2016). Methods for estimating annual exceedance probability discharges for streams in Arkansas, based on data through water year 2013. *Scientific Investigations Report 2016–5081*. U.S. Geological Survey, Reston, VA, 149 p.

Wischmeier, W. H. (1959). A rainfall erosion index for a universal soil-loss equation. *Soil Science Society of America Journal* 23(3), 246–249.

Yitayew, M., Pokrzywka, S. J. and Renard, K. G. (1999). Using GIS for facilitating erosion estimation. *Applied Engineering in Agriculture* 15(4), 295–301.

Zhang, G. H., Nearing, M. A. and Liu, B. Y. (2005). Potential effects of climate change on rainfall erosivity in the Yellow River Basin of China. *Transactions of the American Society of Agricultural Engineers* 48, 511–517.

Zhang, X. C. and Nearing, M. A. (2005). Impact of climate change on soil erosion, runoff, and wheat productivity in Central Oklahoma. *CATENA* 61(2–3), 185–195.

Zingg, A. W. (1940). Degree and length of land slope as it affects soil loss in runoff. *Agriculturists* 21, 59–64.